J. Fluid Mech. (1985), *vol.* 154, *pp.* 337–356
Printed in Great Britain

Forces on cylinders in viscous oscillatory flow at low Keulegan–Carpenter numbers

By P. W. BEARMAN, M. J. DOWNIE, J. M. R. GRAHAM AND E. D. OBASAJU

Department of Aeronautics, Imperial College, London SW7 2BY

(Received 30 June 1983 and in revised form 18 November 1984)

This paper presents a comparison between theory and experiment for the in-line forces on cylinders of general cross-section in planar oscillatory flows of small amplitude. The theoretical analysis evaluates corrections to the standard inviscid inertial force at low Keulegan–Carpenter numbers which arise from the presence of viscous laminar boundary layers and from the development of vortex shedding. The boundary-layer contribution due to both skin friction and displacement effects is calculated to first order in the Stokes parameter $\beta^{-\frac{1}{2}}$. The contribution to the in-line force from separation and vortex shedding, for which the results presented only apply to sharp-edged bodies, is taken from previous work on vortex shedding from isolated edges using the discrete vortex modelling technique. The resulting force has components both in phase with the fluid acceleration (inertia) and in phase with the velocity (drag).

The theoretical results are compared to measurements taken in a U-tube water channel on a number of cylinders of different cross-section including circular cylinders and sharp-edged sections. The comparisons suggest that the theory is valid for Keulegan–Carpenter numbers below about 3 and for moderately high values of the β parameter.

1. Introduction

When a cylindrical body moves with oscillatory motion in a direction perpendicular to its axis, in an otherwise stationary fluid, it experiences a force opposing the motion which may be considered to be composed of three parts: due to the inertia of the accelerating outer flow; due to the influence of viscous boundary layers; and due to separation of these boundary layers leading to the shedding of vortices. If the amplitude of the motion is small compared to the body diameter D, as is the case considered in this paper, the dominant part of the force is the inviscid inertia force. This force is related to the acceleration of the fluid in inviscid attached flow past the cylinder and is the only force present in the limit of very high Reynolds number and very small Keulegan–Carpenter number. For periodic motion the Keulegan–Carpenter number $K_c = \hat{U}_0 T/D$, where $\hat{U}_0$ is the maximum velocity of the body and T is the period of the motion, is proportional to the amplitude of the motion divided by the body diameter. The Reynolds number is defined as $R = \hat{U}_0 D/\nu$, where ν is the kinematic viscosity. When the cylinder is at rest and the fluid is oscillating the inertia force is increased by the Froude–Krylov force, a buoyancy force caused by the pressure gradient imposed on the fluid to generate the oscillating flow. This paper is mainly concerned with the problem of fixed cylinders in oscillating flow and the work has application to the problem of predicting forces on structures subject to water waves.

The second of the three components of the force arises from the influence of viscosity on the attached flow on the body surface through a displacement effect and through the generation of skin friction. This component of force is insignificant for most large structures but may become important in model testing in wave tanks where the Reynolds numbers are significantly smaller than those of the full-scale structure.

For arbitrary body shapes the regime for attached flow will depend on both the Keulegan–Carpenter number and the Reynolds number. In the case of a circular cylinder there is a regime at sufficiently small Keulegan–Carpenter number for which the flow round the body remains attached throughout the motion regardless of the Reynolds number. The analysis for oscillatory viscous flow was first given by Stokes (1851) for the case of spherical and cylindrical pendulum bobs. His solution is given in the form of a series expansion in powers of $\beta^{-\frac{1}{2}}$ where the viscous-frequency parameter $\beta = D^2/\nu T$.

For a circular cylinder moving with velocity $U = \hat{U}_0 \cos \omega t$ where $\omega = 2\pi/T$, in otherwise still fluid, the force F per unit length of the cylinder is

$$F = \tfrac{1}{4}\pi\rho D^2 \omega \hat{U}_0 (k \sin \omega t - k' \cos \omega t), \tag{1}$$

with $$k = 1 + 4(\pi\beta)^{-\frac{1}{2}},$$

and $$k' = 4(\pi\beta)^{-\frac{1}{2}}.$$

Equation (1) shows that viscous effects contribute both to the inertial force, which is the part of the force in phase with acceleration, and to the drag force, which is defined as the part of the force in phase with velocity. Sarpkaya (1981) and Bearman *et al.* (1981) have both discussed the importance of viscous effects at low Keulegan–Carpenter numbers.

Expressing (1) in the form suggested by Morison *et al.* (1950) for wave forces on structures, namely:

$$F = \tfrac{1}{2}\rho U |U| D C_{\mathrm{D}} + \tfrac{1}{4}\pi\rho D^2 \frac{\mathrm{d}U}{\mathrm{d}t} C_{\mathrm{M}}, \tag{2}$$

gives $$C_{\mathrm{M}} = 1 + 4(\pi\beta)^{-\frac{1}{2}} + O(\beta^{-1}),$$

and $$C_{\mathrm{D}} = \tfrac{3}{2}\pi^3 K_c^{-1} (\pi\beta)^{-\frac{1}{2}} + O(\beta^{-1}) \tag{3}$$

for the inertia and drag coefficients. C_{D} is obtained by multiplying each side of (2) by $\cos \omega t$ and integrating over the period of one cycle. This method for obtaining C_{D} which was used originally by Keulegan & Carpenter (1958) will be used throughout this paper.

The viscous parameter β appearing in the above expressions is the ratio of the Reynolds number to the Keulegan–Carpenter number and has been shown by Sarpkaya (1976) to be an important influence on circular-cylinder flow. It is a convenient parameter for periodic oscillatory flows since, for a given model size and fluid, the β parameter depends only on the flow frequency, whereas the Reynolds number depends on flow frequency and oscillation amplitude. In small-scale laboratory tank tests the β parameter typically takes a value in the range 10^2 to 10^3. Hence it can be seen from (1) that the higher-order terms $O(\beta^{-1})$ are likely to be unimportant but that the $\beta^{-\frac{1}{2}}$ terms can make a significant contribution to the force. For this reason calculation of viscous effects is developed in this paper up to $O(\beta^{-\frac{1}{2}})$ and applied to

bodies of general cross-section. This approach (see Graham 1981) follows the earlier analysis of Stuart (given in Rosenhead 1963) but includes boundary-layer displacement effects as well as skin friction.

In the case of a *fixed* circular cylinder in an oscillatory flow the resulting force coefficients are:

$$\left.\begin{aligned} C_{\mathrm{M}} &= 2+4(\pi\beta)^{-\frac{1}{2}} \\ \text{and} \qquad C_{\mathrm{D}} &= \tfrac{3}{2}\pi^3 K_c^{-1}(\pi\beta)^{-\frac{1}{2}} \end{aligned}\right\} \tag{4}$$

These are the same as Stokes' results (3) to $O(\beta^{-\frac{1}{2}})$ except for the additional inviscid inertia component due to the Froude–Krylov force.

The problem of a fixed circular cylinder in oscillatory incompressible viscous flow has also been investigated theoretically by Wang (1968) to $O(\beta^{-\frac{3}{2}})$ using the method of inner and outer expansions. The solution applies to high-frequency oscillating flow of instantaneous velocity $U = \hat{U}_0 \mathrm{e}^{\mathrm{i}t_1}$, for which $S \gg 1$, $RS \gg 1$ and $R/S \ll 1$. Here the frequency parameter $S = \pi K_c^{-1}$ and $t_1 = \omega t$. In the case of an oscillating cylinder in otherwise still fluid, the values of the force coefficients calculated from Wang's results can be shown to agree with (3) to leading order in $\beta^{-\frac{1}{2}}$. In the analogous case of a fixed circular cylinder in oscillatory flow, the result for the in-line force is

$$\frac{F}{\frac{1}{2}\rho \hat{U}_0^2 D} = 2\pi \mathrm{i} S \mathrm{e}^{\mathrm{i}t_1} + 4\pi \left(\frac{S}{R}\right)^{\frac{1}{2}} (1+\mathrm{i})\, \mathrm{e}^{\mathrm{i}t_1} + \frac{4\pi}{R} \mathrm{e}^{\mathrm{i}t_1} + \frac{\pi(1-\mathrm{i})}{R(RS)^{\frac{1}{2}}} \mathrm{e}^{\mathrm{i}t_1} + O(S^{-1}).$$

(Note that, in Wang's original expression, the Reynolds number was half that used here.) This can be expressed, as before, in terms of Morison's equation (2) with force coefficients:

$$C_{\mathrm{D}} = \tfrac{3}{2}\pi^3 K_c^{-1}(\pi\beta)^{-\frac{1}{2}} + \tfrac{3}{2}\pi^2 K_c^{-1}\beta^{-1} - \tfrac{3}{8}\pi^3 K_c^{-1}(\pi\beta)^{-\frac{3}{2}};$$

$$C_{\mathrm{M}} = 2+4(\pi\beta)^{-\frac{1}{2}} + (\pi\beta)^{-\frac{3}{2}}.$$

The theoretical results for the oscillating circular cylinder C_{D} have been tested indirectly by several investigators who measured the decay of the amplitude of vibration of cylindrical pendula. In such experiments, however, the flow is not truly analogous to a cylinder vibrating in a direction normal to its length, partly because it is not two-dimensional, but also, as was pointed out by Stuart & Woodgate (1954), because there is a longitudinal component of acceleration present. A further drawback with this technique is the problem of end effects, which are usually assumed to be negligible providing the length-to-diameter ratio of the pendulum is large. Three-dimensional effects of this type may be eliminated by studying cylinders in true planar motion.

The third component of the force on a body in oscillatory flow arises from separation of the boundary layer and the generation of vortices. Separation occurs on bodies with continuous surface slope when the Keulegan–Carpenter number exceeds some critical value, depending on the Reynolds number (or β parameter) and the local body shape. In the case of a circular cylinder it is usually expected that the onset of vortex shedding occurs at a Keulegan–Carpenter number of about 5, above which a rapid increase in the drag coefficient is observed to take place (see for example Sarpkaya 1976; Sarpkaya & Isaacson 1981). One of the purposes of the present paper is to evaluate the drag coefficient in the neighbourhood of this critical value. However, bodies which have sharp edges apparently do not have any low-Keulegan–Carpenter-number regime for which the flow remains attached unless perhaps when the β parameter is extremely small. If the edge is truly sharp, separation will always occur

at the edge. Such a separation might remain in the form of a closed bubble in low-Reynolds-number unidirectional flow but in oscillatory flow it appears that the action of flow reversal sweeps the detached vorticity out into the fluid to form a shed vortex.

When the separation points are known an inviscid analysis can be used to give a reasonable prediction of the force F_v induced by vortex shedding. This type of calculation was carried out by Graham (1980) for the force induced on an isolated sharp edge in oscillatory flow. The method of calculating this force involved modelling the separating shear layers, which feed the growing vortices, by the discrete-point-vortex method. The vortex force was found from this analysis to be proportional to K_c raised to a power depending on the internal angle δ of the edge. The resulting forms for the coefficients in Morison's equation are

$$\left.\begin{aligned} C_{\mathrm{M}} &= C_{\mathrm{M0}} + B_{\mathrm{e}} K_c^{2\pi/(3\pi-2\delta)} \\ \text{and} \quad C_{\mathrm{D}} &= A_{\mathrm{e}} K_c^{(2\delta-\pi)/(3\pi-2\delta)}, \end{aligned}\right\} \tag{5}$$

where C_{M0} is the inviscid inertia coefficient for attached flow. The factors A_{e} and B_{e} were calculated, for different values of edge angle, by using the discrete vortex method. These results have been used in the present paper to compute separated flow-force coefficients for three sharp-edged bodies: a square section face on to the flow, a square section diagonally on to the flow and a thin flat plate with edge angles of 60°.

A corresponding series of force measurements have been carried out on similar bodies in planar oscillatory flow. The flow is kinematically the same in these tests as that around a corresponding oscillating body in otherwise still fluid. Results will be presented for the streamwise force on sharp-edged cylinders and circular cylinders. At the values of β used in these experiments the square-section cylinders are subject to a small viscous contribution to the overall in-line force. It is possible, as in the case of the circular cylinder, to calculate this force to $O(\beta^{-\frac{1}{2}})$ by using boundary-layer theory and assuming attached flow. The results of these computations will be presented. However, it is clear that except at the very lowest Keulegan–Carpenter numbers, where separation effects on the body are confined to small regions surrounding each edge, attached flow will not give an adequate prediction of the inviscid surface velocity, and hence of the boundary-layer thickness. Hence the viscous-force prediction is likely to be considerably in error for these cases. In this sense the three parts of the force under consideration interact with one another.

The present paper compares predicted in-line forces, for the three sharp-edged sections listed above and for the circular cylinder with measurements made in oscillatory flow in a U-tube. The aim is to establish the behaviour of the force coefficients, C_{M} and C_{D}, at very low K_c, where at present there is little or no experimental data available, and to provide a means of checking the validity of the attached viscous- and separated inviscid-flow theories.

2. Experimental arrangement and presentation of results

The measurements were made in the planar oscillatory flow generated in a U-tube water tunnel. The working section of the U-tube, which is in the horizontal limb, is 0.61 m square and 1.5 m long. The vertical arms are 2.5 m high. Constant-amplitude oscillations are maintained by an air blower, attached to one of the vertical limbs, which is switched on and off at appropriate intervals by the signal from a capacitance

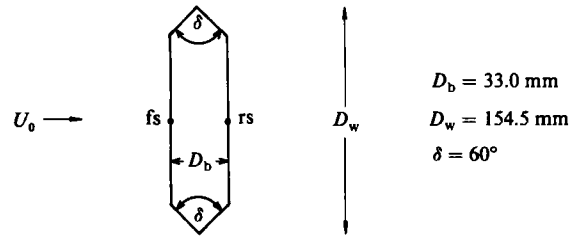

(*a*) the plate

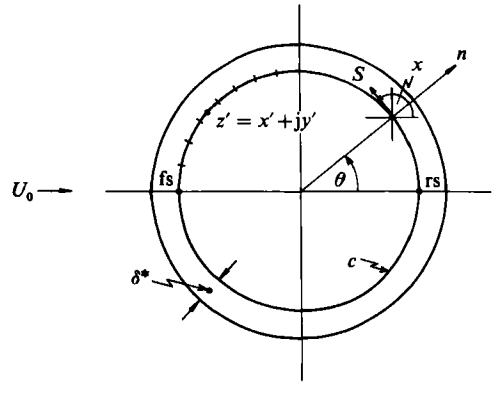

(*b*) the circular cylinder

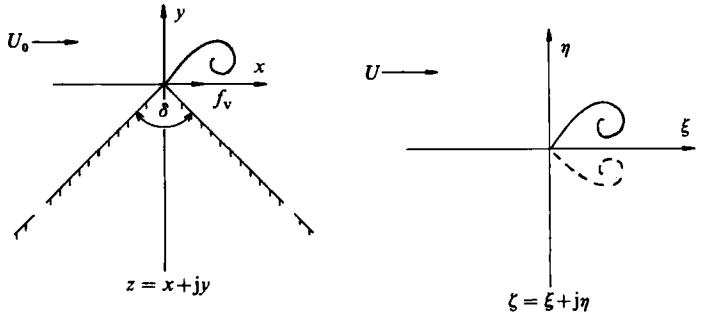

(*c*) the isolated edge

FIGURE 1. Notation and geometry of bodies: (*a*) the plate; (*b*) the circular cylinder; (*c*) the isolated edge.

gauge recording the instantaneous water level. When the tube is filled to the working-level mark, the period T of the oscillation of the water is 3.34 s and the displacement of the surface can be varied up to 0.6 m peak-to-peak.

Six sizes of circular cylinder, a flat-plate model and a sharp-edged square-section cylinder were tested. The circular-cylinder diameters varied from 2.56 to 7.48 cm, giving a viscous parameter β ranging between 196 and 1665. The length of a side of the square-section cylinder was 2.67 cm, giving a value for β of 213 when face on to the flow. The same cylinder tested with one diagonal parallel to the flow (hereinafter referred to as the diamond) gave a value for β of 432. The plate was 3.84 cm wide

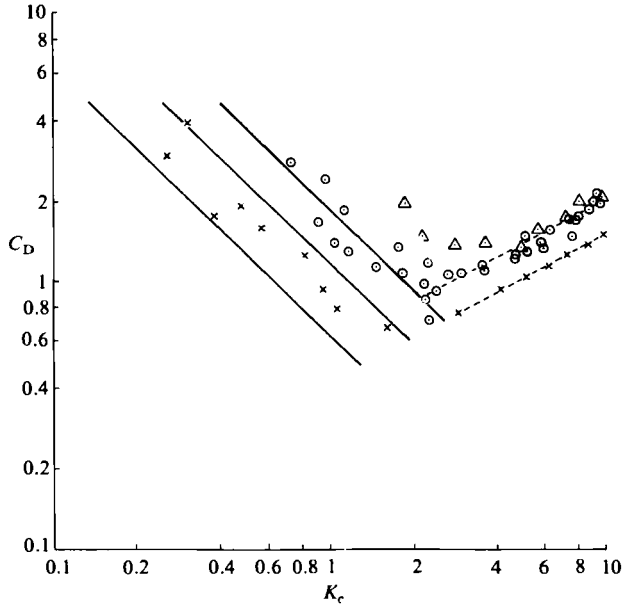

FIGURE 2. Drag coefficient *vs.* Keulegan–Carpenter number for circular cylinder. Experiment: ×, $\beta = 1665$; ⊙, 483; △, 196.

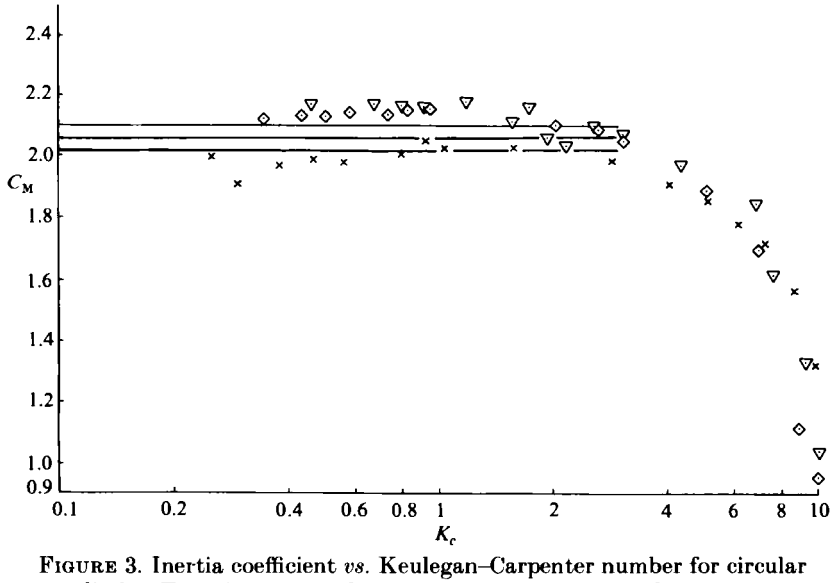

FIGURE 3. Inertia coefficient *vs.* Keulegan–Carpenter number for circular cylinder. Experiment: ×, $\beta = 1665$; ◇, 1204; ▽, 964; theory, ——.

and was set normal to the flow, giving a value for β of 439. The plate, which is shown in figure 1(*a*), was machined from a thin rectangular section and the edges were chamfered to give a 60° internal angle. Tests were carried out over values of K_c ranging from 0.1 to 10. The Reynolds number varied between 350 and 16650 for the range of β and K_c used.

Each model was 60.5 cm long and mounted horizontally, being supported at each end on strain-gauged load cells let into the walls of the U-tube. Water level and in-line

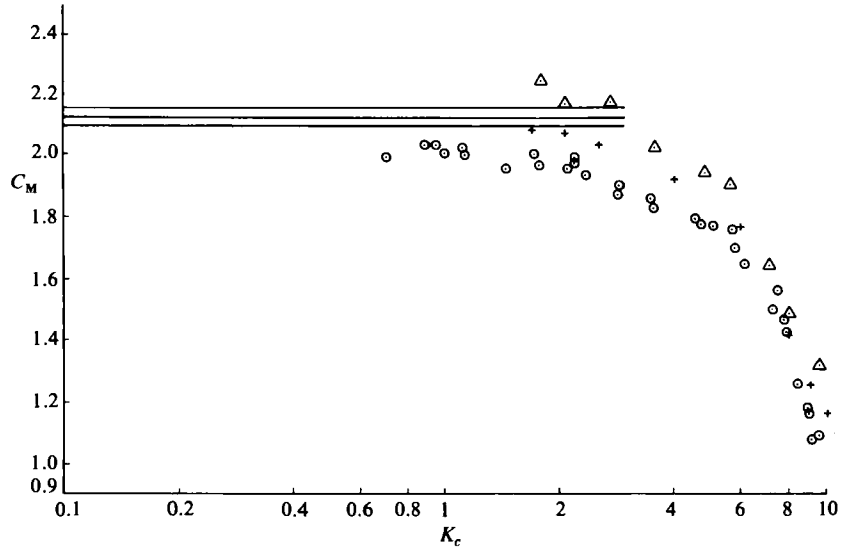

FIGURE 4. Inertia coefficient *vs.* Keulegan–Carpenter number for circular cylinder. Experiment: ⊙, $\beta = 483$; +, 301; △, 196; theory, ——.

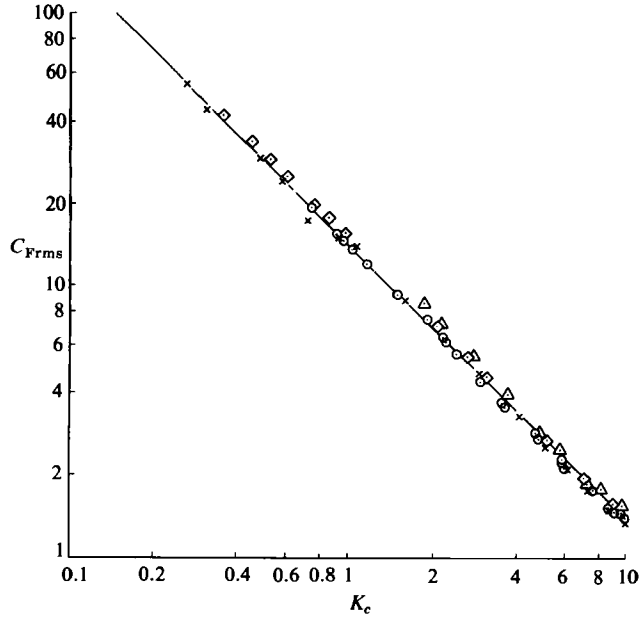

FIGURE 5. In-line force coefficient *vs.* Keulegan–Carpenter number for circular cylinder. Experiment: ×, $\beta = 1665$; ◇, 1204; ⊙, 483; △, 196; theory: ($C_{Frms} = \sqrt{2}\,\pi^2/K_c$).

force signals were recorded simultaneously on analog tape, and then discretized and processed on a digital computer. The sampling rate was such that one cycle of the water-level oscillation was defined by 420 data points. The in-line force was analysed according to Morison's equation (2) and C_D and C_M were calculated from the average of 50 cycles of data. The force coefficients for the circular cylinder are presented in figures 2, 3 and 4, plotted against K_c. An alternative way of presenting these results

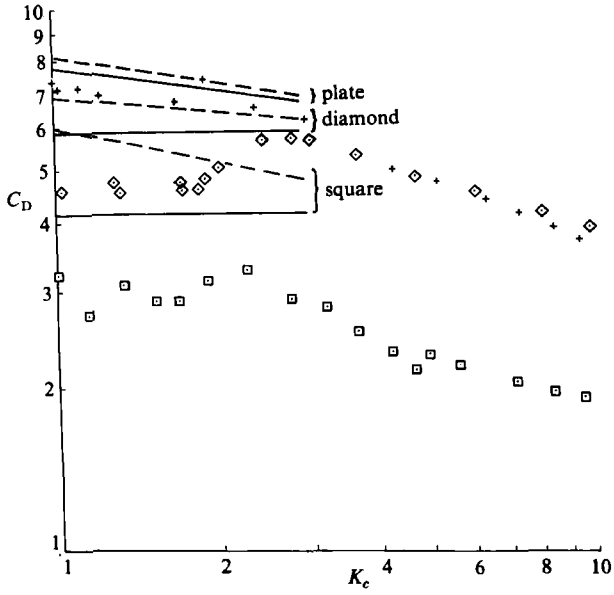

FIGURE 6. Drag coefficient *vs.* Keulegan–Carpenter number for sharp-edged cylinders. Experiment: +, flat plate ($\delta = 60°$), $\beta = 439$; ◇, diamond (90°), 431; ⊡, square (90°), 231. Theory: ——, isolated edge theory C_{Dv}; – – –, isolated edge theory plus viscous correction $C_{Dv} + C_{DBL}$.

is to calculate the root-mean-square value and the phase angle of the force. The relationship between the r.m.s. in-line force, normalized with respect to $\frac{1}{2}\rho \hat{U}_0^2 D$, and the Morison force coefficients may be shown to be (see e.g. Bearman & Graham 1979):

$$C_{Frms} = (\tfrac{3}{8}C_D^2 + \tfrac{1}{2}\pi^4 K_c C_M)^{\frac{1}{2}}. \tag{6}$$

The results for C_{Frms} are shown in figure 5 plotted against K_c. The behaviour of the force coefficients with varying K_c for the sharp-edged cylinders is represented in figures 6 and 7.

3. Calculation of the forces induced on a body in oscillatory flow

3.1. *Attached flow*

The effect of the Stokes boundary layers on an arbitrary cylindrical body in oscillatory cross-flow is analysed in the Appendix. Provided the Reynolds number of the flow is sufficiently large, K_c is small and the flow remains attached, the concept of a boundary layer perturbing an outer inviscid flow is valid. In that case the additional force due to skin friction and the effect of the boundary-layer displacement thickness is given by (A 2) as:

$$F_{BL} = \frac{(1+\mathrm{i})\rho\omega D}{(\pi\beta)^{\frac{1}{2}}} \oint_S q_{e0}\,\mathrm{d}x. \tag{7}$$

q_{e0} is the flow speed on the body surface S calculated by inviscid theory, and F_{BL} is the component of force aligned with the free stream (x-axis). The integral and q_{e0} are both defined to be positive in the anticlockwise sense round the body.

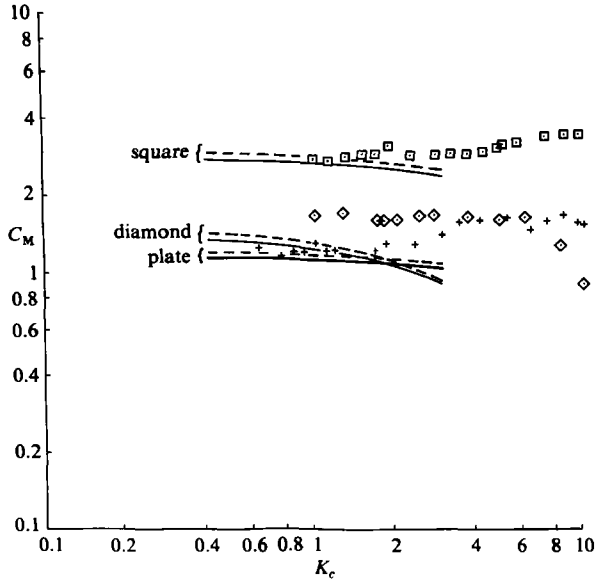

FIGURE 7. Inertia coefficient *vs.* Keulegan–Carpenter number for sharp-edged cylinders. Experiment: +, flat plate, $\beta = 439$; ◇, diamond, 431; □, square, 231. Theory: ——, isolated edge theory ($C_{M0} + C_{Mv}$); ---, isolated edge theory plus viscous correction ($C_{M0} + C_{Mv} + C_{MBL}$).

In the case of a circular cylinder in oscillatory flow

$$\hat{q}_{e0} = -2\hat{U}_0 \sin\theta, \quad \hat{F}_0 = \tfrac{1}{2}i\omega\rho\hat{U}_0 \pi D^2,$$

and

$$\left.\begin{aligned} \hat{F}_{BL} &= \frac{(1+i)\rho\omega D}{(\pi\beta)^{\frac{1}{2}}} \int_0^{2\pi} 2\hat{U}_0 \sin^2\theta \, \tfrac{1}{2}D \, d\theta \\ &= (1+i)\rho\omega\hat{U}_0 D^2 \left(\frac{\pi}{\beta}\right)^{\frac{1}{2}}. \end{aligned}\right\} \tag{8}$$

The drag and inertia coefficients may be found by considering the real and complex parts (with respect to time) of the in-line force. Using the definition of Morison's equation:

$$C_D = \tfrac{3}{8}\pi \frac{\mathrm{Re}\{\hat{F}\}}{\tfrac{1}{2}\rho\hat{U}_0^2 D};$$

$$C_M = \frac{4}{\pi} \frac{\mathrm{Im}\{\hat{F}\}}{\rho\omega\hat{U}_0^2 D};$$

the force coefficients are

$$\left.\begin{aligned} C_D &= \tfrac{3}{2}\pi^3 K_c^{-1}(\pi\beta)^{-\frac{1}{2}}, \\ C_M &= 2 + 4(\pi\beta)^{-\frac{1}{2}}. \end{aligned}\right\} \tag{9}$$

These results have already been compared with those obtained by Stokes (see (3)) in the introduction. They are plotted, together with the experimental results, in figures 2–4. If the results are substituted in (6), it may be seen that

$$C_{F\mathrm{rms}} = \sqrt{2}\,\pi^2 K_c^{-1}\{1 + 2(\pi\beta)^{-\frac{1}{2}}\}.$$

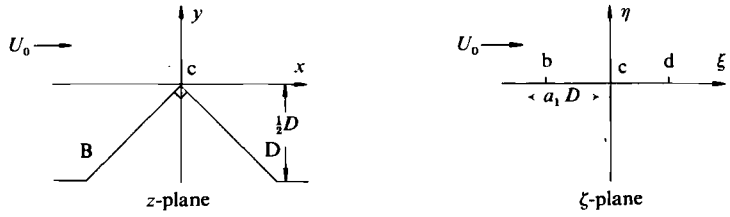

$$z = \int_0^{\zeta} \frac{\zeta^{\frac{1}{2}}}{(\zeta^2 - \zeta_d^2)^{\frac{1}{2}}} d\zeta \qquad a_1 = 0.835$$

(*a*) transformation for diamond

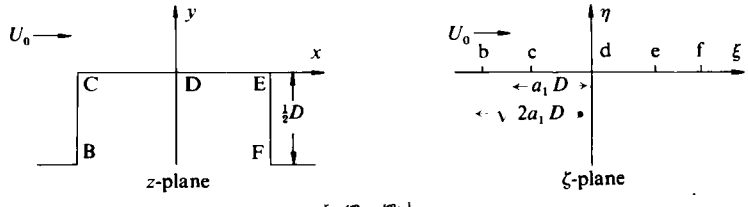

$$z = \int_0^{\zeta} \left(\frac{\zeta^2 - \zeta_e^2}{\zeta^2 - \zeta_f^2} \right)^{\frac{1}{2}} d\zeta$$

(*b*) transformation for square

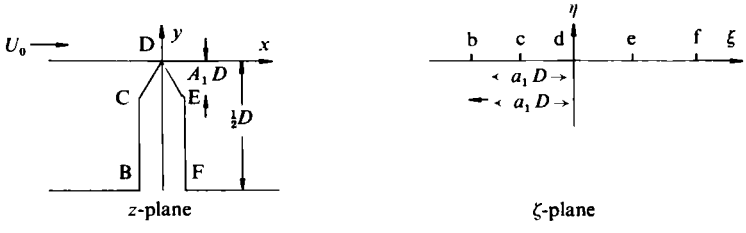

$A_1 = 0.16$ $\qquad \int_0^{\zeta} \frac{(\zeta^2 - \zeta_e^2)^{\frac{1}{2}} \zeta^{\frac{1}{2}}}{(\zeta^2 - \zeta_f^2)^{\frac{1}{2}}} d\zeta \qquad a_1 = 0.407$ and 0.54

(*c*) transformation for plate

FIGURE 8. Conformal transformations for sharp-edged bodies.

For large β, C_{Frms} approaches its inviscid value. This occurs because the in-line force is dominated by the inertia component, and the inertia coefficient tends towards its value for inviscid flow. The inviscid value of C_{Frms}, given by the curve $C_{\mathrm{Frms}} = \sqrt{2}\,\pi^2 K_c^{-1}$, has been plotted against K_c and is shown along with the experimental results in figure 5.

In the case of the sharp-edged cylinders, the force coefficicnts may be most easily obtained by considering the flow in the transformed plane. The half bodies and their transformation are shown in figure 8. The tangential velocity is related to the complex potential $W = U_0 \zeta$ by the expression

$$q_{\mathrm{e}}\, \mathrm{e}^{-\mathrm{j}\chi(s)} = -\frac{\mathrm{d}w}{\mathrm{d}z} = -\hat{U}_0 \frac{\mathrm{d}\zeta}{\mathrm{d}z},$$

Body	a_1	$Re(A_{BL})$	$\beta^{\frac{1}{2}}K_c C_{DBL}$	$\beta^{\frac{1}{2}}C_{MBL}$
Diamond	0.385	$2(-a1)/\sqrt{2}$	19.73	1.70
Square	0.835	$-a1+(-a1)$	27.00	2.40
Plate	0.407	$2(-a1)/2$	6.80	0.59

TABLE 1. Force coefficients due to presence of boundary layer

where $\chi(s)$ is the orientation of the body surfacc in the positive s-direction. If the force component F_{BL} is given by the real part of the complex force $\mathscr{F}_{BL}$, then, from (A 2) in the Appendix,

$$\mathscr{F}_{BL} = -\frac{(1+i)}{(\pi\beta)^{\frac{1}{2}}}\rho\omega D \oint_S \hat{U}_0 \frac{d\zeta}{dz} e^{i\chi}\, dz.$$

Therefore,

$$\mathscr{F}_{BL} = -\frac{(1+i)}{(\pi\beta)^{\frac{1}{2}}}\rho\omega D\hat{U}_0 \int_c e^{i\chi}\, d\zeta.$$

For a body that is symmetrical about the direction of flow,

$$\mathscr{F}_{BL} = -\frac{2(1+i)}{(\pi\beta)^{\frac{1}{2}}}\rho\omega D\hat{U}_0 \int_{rs}^{fs} e^{i\chi}\, d\zeta,$$

$$= -4(\pi)^{\frac{1}{2}}\frac{(1+i)}{K_c(\beta)^{\frac{1}{2}}}\rho\hat{U}_0^2 D A_{BL},$$

where

$$A_{BL} = \sum_{k=1}^{N+1}(a_{k+1}-a_k)\, e^{i\chi}_k.$$

$(a_k D, 0)$ are the coordinates in the transformed plane of the N edges of the bodies numbered consecutively from the rear to the front stagnation points. The in-line force component F_{BL} is given by the real part (with respect to space) of $\mathscr{F}_{BL}$ and the viscous-force coefficients are given by the real and imaginary parts of F_{BL} with respect to time:

$$\left.\begin{aligned} C_{DBL} &= -3\pi^3 K_c^{-1}\,\mathrm{Re}\{A_{BL}\}(\pi\beta)^{-\frac{1}{2}}; \\ C_{MBL} &= -\frac{8}{\pi}\,\mathrm{Re}\{A_{BL}\}(\pi\beta)^{-\frac{1}{2}}; \end{aligned}\right\} \tag{10}$$

based on the diameter of the circumscribing circle. The calculation for the in-line viscous force coefficients for the sharp-edged cylinders is summarized in table 1. The resulting overall force coefficients are shown in figures 6 and 7 along with the experimental results.

3.2. *The force due to vortex shedding*

In the case of sharp-edged cylinders, flow separation occurs even at low K_c. The component F_v of the in-line force associated with the resulting vortex shedding contributes to both the inertia force and the drag force. The force may be calculated by a technique involving the matching of the flows in the near vicinity of the cylinder shedding edges with the local oscillatory separated flow in the immediate neighbourhood of an isolated edge (Graham 1980).

The flow about an infinite wedge in the z-plane (see figure 1 *c*) was computed using

a discrete vortex calculation in a transformed plane, the ζ-plane, in which the wedge was opened out into a plane wall. The Schwartz–Christoffel transformation that was used is given by

$$Z = \mathrm{e}^{\mathrm{j}a\pi} L^{(1-\lambda)} \zeta^{\lambda}, \tag{11}$$

where a determines the edge orientation, L is a lengthscale implied by the transformation, and λ is related to the internal angle by $\lambda = 2 - \delta/\pi$. Point vortices were shed sequentially from the edge and tracked as they moved with the fluid in oscillatory flow. Groups of vortices which could be identified as representing completely rolled-up sheets far from the body were progressively wound into central-core vortices. Each fully formed vortex shed was found to pair, either with a vortex shed in the previous half cycle, or with its own image, and as a result to move rapidly away from the edge. The calculation was found to be limited to internal edge angles less than about 120°, beyond which it ceased to give realistic shedding patterns.

The main results obtained from the isolated edge analysis were as follows. The vortex force f_{v} was found to be directed at right angles to the edge-angle bisector (for bodies symmetric about that bisector) and given by

$$f_{\mathrm{v}}(t) = \tfrac{1}{2}\rho \hat{U}_0^2 L K_c^{(3-2\lambda)/(2\lambda-1)} \Psi(t), \tag{12}$$

where Ψ is a dimensionless function of time obtained from the numerical computation. The Morison equation in-line force coefficients were determined via (5), with the values of A_{e} and B_{e} given by

$$A_{\mathrm{e}} = \frac{3\pi}{4T} \int_0^T \Psi \sin \omega t \, \mathrm{d}t,$$

$$B_{\mathrm{e}} = \frac{2}{\pi^2 T} \int_0^T \Psi \cos \omega t \, \mathrm{d}t,$$

calculated from the discrete-vortex simulation taking cyclic averages over 5 cycles of computed flow. In order to avoid any starting transients the averages were taken typically between the fifth and ninth cycles after the commencement of the motion.

In a real flow at low K_c the maximum displacement of particles in the undisturbed flow is small compared to the scale of the body. It is therefore impossible for vortices to move far from the edge of the body from which they are shed except under the induced velocity field of other vortices, and shedding at any edge becomes independent of the other edges. Thus, at low K_c the shedding from a single edge of a body, providing it is sufficiently far removed from all other edges of the body for there to be no mutual interference, is analogous to the case of shedding from an isolated edge. The vortex-induced forces on a sharp-edged body, then, may be found directly from the results of the isolated-edge calculation by simply matching the local flow around each shedding edge of the body with the local flow about the isolated edge, and summing their contributions. Such a procedure has been carried out in the present work for the cases of the square, the diamond and the flat plate of finite thickness with chamfered edges.

The circular cylinder was excluded partly because the isolated-edge analysis is not strictly applicable (since in this particular case one of the assumptions concerning the behaviour of the far-field vortices cannot formally be shown to hold) and partly because the separation lines are not fixed and are very difficult to predict in oscillating flow.

Body	λ	$\lambda e^{i\alpha\pi} E$	N	a_L	n_x	A_e	B_e	C_{Dv}	C_{Mv}
Diamond	$\frac{3}{2}$	$(-\zeta_d)^{-2}$	2	1.878	1	1.566	−0.157	5.882	−0.590
Square	$\frac{3}{2}$	$(2\zeta_d)^{\frac{1}{2}}(\zeta_d^2-\zeta_e^2)^{-\frac{1}{2}}$	4	0.939	$\sqrt{2}$	1.566	−0.157	4.159	−0.417
Plate	$\frac{5}{3}$	$(-\zeta_e^2)^{\frac{1}{3}}(-\zeta_f^2)^{-\frac{1}{3}}$	2	1.489	1	2.602	−0.014	7.761	−0.042

TABLE 2. Force coefficients due to vortex shedding

The half bodies and their transformations are shown in figure 8. In the near vicinity of the shedding edge z_e, as $z \to z_e$, the transformation takes the form

$$z \to e^{j\alpha\pi} E \zeta^{\lambda},$$

where E is determined by the body geometry. Thus, very close to the shedding edge, the local transformations are identical with the transformation for the isolated edge (see (11)) providing that the internal angles are the same, and also that

$$L^{(1-\lambda)} = E.$$

If the transformations are identical, and if the velocity U_0 in the body transformed plane is the same as that in the transformed plane for the isolated edge, then the two edge flows U_e in the real plane must be identical since

$$U_e = U_0 \frac{d\zeta}{dz}\bigg|_{z \to z_e}.$$

The edge flows are matched, then, provided that the ratio a_L of the lengthscales is given by

$$a_L = \frac{L}{D} = \frac{E^{1/(1-\lambda)}}{D},$$

where D is the characteristic length of the body.

The vortex force in-line with the direction of the free stream is $f_v n_x$, where n_x is its direction cosine with respect to the x-axis, which is always parallel to the direction of the free stream. Since the vortex force on the isolated edge is proportional to the lengthscale L (see (12)) the in-line force coefficients for a body with edges of the same angle may now be written in terms of the isolated edge results as:

$$C_D = \sum_{k=1}^{N} a_{Lk} n_{xk} A_e K_c^{(3-2\lambda)/(2\lambda-1)},$$

$$C_M = \sum_{k=1}^{N} a_{Lk} n_{xk} B_e K_c^{2/(2\lambda-1)},$$

where N is the number of shedding edges on the body.

The calculations for the three bodies in question are summarized in table 2 and the results are presented in full in figures 6 and 7, where the experimental results are also plotted.

4. Discussion of results

The behaviour of the drag coefficient with varying β is shown for the circular cylinder over a range of K_c from 0.1 to 10.0 in figure 2. It may be seen that, for a given value of K_c, the drag coefficient drops as the β parameter increases. More striking,

perhaps, is the change in trend with K_c exhibited by the data. As K_c increases from a value of 0.1, the drag coefficient first decreases with increasing K_c until a given value of K_c (depending on the β parameter, but somewhere in the region of 2) is approached. In this region the viscous-flow theory predicts values of the drag coefficient in approximate agreement with those obtained from experimental results. As K_c increases beyond this region, the drag coefficient rises.

At very low K_c the flow is unseparated and a regime in which viscous effects dominate is to be expected. As K_c increases the boundary layers separate and, at a sufficiently high value, a regime in which the flow is dominated by vortex shedding is established. The occurrence of these two distinct regimes in the K_c range covered in the present investigation has been indicated by previous studies. Measurements by Stuart & Woodgate (1954) suggested that the viscous regime for circular cylinders occurs for amplitudes of vibration of about one tenth or less of the cylinder diameter, i.e. $K_c \lesssim 0.6$. Flow-visualization experiments carried out by Singh (1979), Grass & Kemp (1979) and Williamson (1982) demonstrate that vortices begin increasingly to dominate the flow for $K_c \gtrsim 5$. It is tempting to assume that the change in trend shown by the force coefficients is attributable to the onset of vortex shedding. This would imply that the initiation of vortex shedding is not associated with a fixed ratio of flow amplitude to cylinder diameter, but depends on the β parameter, since the change of trend occurs at different values of K_c with different values of β.

A better estimate of the effect of vortex shedding may be obtained by subtracting the theoretical value of the viscous drag coefficient $C_{\mathrm{D_{BL}}}$ (see (9)) from the drag coefficient obtained from the experimental data, as shown in figure 9. Extrapolating these results (dashed line) suggests that the additional contribution to the drag force tends linearly to zero. But the scatter at lower values, probably due to inaccuracies in the measurement of the forces, which are very small, may obscure a region $K_c < K_{cv}$ in which there is no contribution from separation. Even if this is so, K_{cv} is small ($\lesssim 1.0$). Applying the separated flow analysis for an isolated edge in oscillatory flow to the case of a circular cylinder, $\delta = \pi$ and therefore $\lambda = 1$, gives:

$$C_{\mathrm{D}} \propto K_c.$$

This result is in agreement with the linear trend of the data in the above figure. However, as discussed above, the analysis cannot be justified for the case when separation is from a smooth surface, so the agreement here may be fortuitous. There is no evidence available to us from flow visualization that separation with vortex shedding occurs on a circular cylinder at such low values of K_c ($\simeq 1$). The increasing $C_{\mathrm{D_v}}$ just above this value may be attributed to the onset of separations which remain attached to the surface as separation bubbles.

The variation of the inertia coefficient for the circular cylinder with the β parameter and K_c is shown in figures 3 and 4. For all values of β the inertia coefficient increases rapidly as K_c decreases from a value of 10.0, until it levels off at a relatively steady value for K_c below about 2.0 or 3.0. In the low-K_c range the increase in the inertia coefficient due to viscous effects is quite evident in the measured data except for the cases $\beta = 483$ which does not appear to be approaching the theoretical level. (It is difficult of course to measure forces very accurately on small cylinders at values of $K_c \sim 1$.)

The variation of drag coefficient with K_c for the sharp-edged cylinders is shown in figure 6. These results are in each case for only one value of β. However, they demonstrate the strong effect of the cross-sectional shape of the cylinder on the force coefficients at low values of K_c. The theoretical results are shown for the inviscid drag

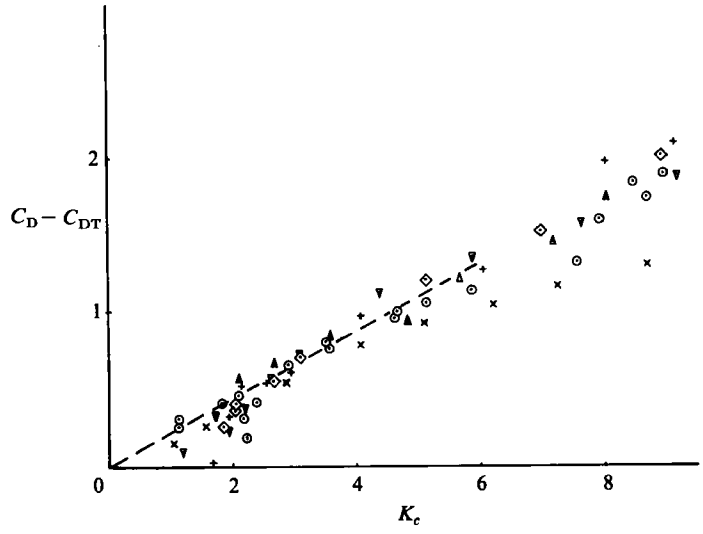

FIGURE 9. Inviscid drag coefficient ($C_D - C_{DT}$) *vs.* Keulegan–Carpenter number for circular cylinder: C_{DT} – Viscous theory value of C_D. ×, $\beta = 1665$; ◇, 1204; ▽, 964; ⊙, 483; +, 301; △, 196.

coefficient C_{D_v}, derived from the matched isolated-edge theory, and the overall drag coefficient associated with the combined inviscid (separated) and viscous (attached) contributions to the in-line force.

The matched-isolated-edge theory assumes that vortices are small compared to the distance between the separation points and, hence, that there is no interaction between the vortices shed from different edges of the cylinder. Flow-visualization experiments (Singh 1979) have shown that, if K_c is much larger than about 3, the size of the vortices is of the order of D and that, particularly in the case of the square, there may be strong interaction between the vortices shed from different edges. The inviscid drag coefficient, therefore, is not expected to be applicable beyond this range. Furthermore, no allowance is made for the effects of viscous diffusion in the discrete-vortex calculation. Pairs of contra-rotating vortices remote from the cylinder are assumed to make a negligible contribution to the in-line force. The effects of viscous diffusion, therefore, may only be expected to significantly affect the calculation in so far as they relate to the forming vortices. Viscous diffusion facilitates the cancellation of oppositely signed circulation in vortex pairs. Its likely effect, which will be more pronounced as β gets smaller, will be the reduction of the vortex force on the body. The present calculation, then, particularly in those cases in which the newly formed but as yet unpaired vortices closely approach the cylinder surface, may be expected to overpredict the vortex force.

The theoretical value of the inviscid drag coefficient may be seen to be in good agreement with experimental results in the case of the plate, although it is about 20 % too high in the cases of the diamond and the square. However, even in the latter two cases the experimental trends are in good agreement with the trends predicted by theory – namely, the drag coefficient is independent of K_c for right-angled shedding edges and, further, the ratio of the drag coefficients for the diamond and the square is $\sqrt{2}$, as predicted by the theory.

The contribution made by the viscous effects in every case raises the value of the drag coefficients, although by a much smaller amount in the case of the plate. The cross-sectional aspect ratio (i.e. the width D_w normal to the flow direction divided

by the streamwise cylinder thickness D_b) is 5.0 compared to a value of 1.0 for the square and the diamond. The contribution made by the skin friction and boundary-layer displacement to the in-line force, depends mainly on the thickness D_b of the cylinder, whereas the contribution made by the pressure forces due to separation depends mainly on the width D_w. Therefore, the viscous contribution forms a much smaller proportion of the overall in-line force in the case of the plate than in the cases of the square and the diamond. Furthermore, in the latter two cases, a larger proportion of the cylinder surface is exposed to local regions of high velocity induced by vortices. In the vicinity of the shedding edge, the direction of the boundary-layer flow may actually be the reverse of that assumed by the viscous theory and, hence, the skin-friction effect will be incorrectly predicted.

The variation of the inertia coefficient with K_c for the sharp-edged cylinders is shown in figure 7. The values of the inviscid attached-flow inertia coefficients C_M of 1.17, 2.80 and 1.80 respectively for the plate, the square and the diamond, were calculated by the boundary integral method (Drossopoulos 1980). Although the magnitude of the inertia coefficients is reasonably well predicted, except perhaps in the case of the diamond, the trend compared with experimental data is disappointing.

When K_c is higher than about 3, it is interesting to note that the trend of the experimental results changes, and the data for C_D appear to lie on curves proportional to $K_c^{-\frac{1}{3}}$ for all sharp-edged cylinders. This may be coincidental but if not it suggests that as the amplitude of the motion increases the fine detail of the cylinder geometry may become much less significant and that as a result a common vortex-shedding pattern ensues.

5. Conclusions

A viscous-flow analysis to $O(\beta^{-\frac{1}{2}})$ has been presented for the drag and inertia coefficients, C_D and C_M respectively, of the in-line force on stationary cylinders of different cross-sections in planar oscillatory flow. The analysis assumes that the Keulegan–Carpenter number K_c is small and that the flow is attached, laminar and two-dimensional.

Force measurements taken on circular cylinders show that the theory gives generally good predictions of the magnitude of these coefficients in the low-Keulegan–Carpenter-number range $K_c < 2.0$. In the higher-Keulegan–Carpenter-number range, the drag coefficient is found to be directly proportional to the Keulegan–Carpenter number if the viscous contribution is first subtracted, whilst the inertia coefficient decreases rapidly with increasing Keulegan–Carpenter number.

In the case of the circular cylinder, the onset of separation effects appears at Keulegan–Carpenter numbers below 1.0.

An inviscid theory is used to calculate the in-line force on three sharp-edged cylinders, namely a thick 'flat plate' with 60° shedding-edge angles, a square-section cylinder with its face normal to the flow, and a diamond cylinder. The theory is claimed to be valid when the Keulegan–Carpenter number is less than about 3. In this range, measurements of the drag and inertia coefficients show that for the case of the flat plate good theoretical predictions are achieved. In the cases of the square and the diamond cylinders, the measured drag coefficients follow the predicted trends, but the theory overpredicts the magnitude of the coefficients by about 20%. The prediction of the inertia coefficient is reasonable in the case of the square, but is less so in the case of the diamond.

When the Keulegan–Carpenter number is larger than about 3, the measured drag

coefficients for all the sharp-edged cylinders vary similarly with Keulegan–Carpenter number suggesting that all the cylinders may have a similar vortex-shedding pattern.

The support of the Science and Engineering Research Council Marine Technology Directorate is gratefully acknowledged.

We are grateful to one of the referees of the first version of this paper for pointing out an error in the boundary-layer analysis.

Appendix. The forces due to the boundary layers on a body in oscillatory flow

We assume that K_c is very small and that the Reynolds number is sufficiently large that the flow can be represented by an outer inviscid flow and an inner viscous laminar boundary layer. Apart possibly from the immediate neighbourhood of a sharp edge, if any are present, the flow is attached. The outer inviscid (zero-order) solution may be obtained by solving Laplace's equation for the complex velocity potential for oscillatory flow past the body. Let the resulting potential be $W_0(z)$, where z is the complex coordinate $x+\mathrm{j}y = re^{\mathrm{j}\theta}$ and $\mathrm{j} = \sqrt{-1}$. This solution has the following properties: $\partial W_0/\partial z \to \hat{U}_0 e^{i\omega t}$, the oscillatory free stream as $r\to\infty$ and $\mathrm{Im}(W_0) =$ constant (usually 0) on the surface S of the body. Let $|\partial W_0/\partial z| = q_{e0} = \hat{q}_{e0} e^{i\omega t}$ be the inviscid surface velocity on S.

In response to this velocity a zero-order oscillatory boundary layer develops on the surface of the body. In the limit $K_c \to 0$ the velocity $q_1 = \hat{q}_1 e^{i\omega t}$ in this boundary layer satisfies:

$$\frac{\partial q_1}{\partial t} = -\frac{1}{\rho}\frac{\partial p_0}{\partial s} + \nu\frac{\partial^2 q_1}{\partial n^2} + O(\beta^{-\frac{1}{2}})$$

with

$$\frac{\partial q_{e0}}{\partial t} = -\frac{1}{\rho}\frac{\partial p_0}{\partial s}, \tag{A 1}$$

where (s, n) are local streamline coordinates (see figure 1*b*). The equation for the high-frequency oscillatory boundary layer has the solution (Batchelor 1967)

$$\hat{q}_1(s, n) = \hat{q}_{e0}(s)\{1 - e^{-(1+\mathrm{i})\alpha n}\},$$

satisfying $q_1 = 0$ on $n = 0$ (the surface of the body) and $q_1 \to q_{e0}$ as $n\to\infty$. q and s are taken as being positive in the anti-clockwise direction round the body and

$$\alpha = \left(\frac{\omega}{2\nu}\right)^{\frac{1}{2}} = \frac{(\pi\beta)^{\frac{1}{2}}}{D}.$$

This boundary layer has a displacement thickness

$$\delta^* = \int_0^\infty \left(1 - \frac{q_1}{q_e}\right) \mathrm{d}n = (1+\mathrm{i})^{-1}\alpha^{-1}$$

which causes an $O(\beta^{-\frac{1}{2}})$ inviscid perturbation $W_1(z)$ to the velocity potential of the outer flow. By considering the effect of δ^* as a source density distribution $m_1(s) = 2\,\mathrm{d}/\mathrm{d}s(q_{e0}\delta^*)$ over the surface S of the body, $W_1(z)$ can be calculated to be

$$W_1(z) = \frac{1}{\pi(1+\mathrm{i})\alpha}\oint_S \frac{\mathrm{d}\hat{q}_{e0}}{\mathrm{d}s}\log(z - z'(s))\,\mathrm{d}s,$$

where $z'(s)$ is a complex coordinate on the surface S. This completes the flow to $O(\beta^{-\frac{1}{2}})$,

which, see Wang (1968), contains no effect of curvature on the boundary layer nor of steady streaming to this order.

The corresponding composite velocity field is

$$(u-jv) = \frac{\partial W_0}{\partial z} + \frac{\partial W_1}{\partial z} + (q_1 - q_{e0})\,e^{-j\chi},$$

where χ is the surface slope of S. It should be noted that, while the surface stream function $\mathrm{Im}\,(W_0)|_S = \text{constant}$, $\mathrm{Im}\,(W_1)|_S = q_e\,\delta^* \neq \text{constant}$, due to the displacement effect of the boundary-layer sources.

In the case of oscillatory flow past a circular cylinder of diameter D the composite flow field to $O(\beta^{-\frac{1}{2}})$ written in terms of the stream function is

$$\psi = \hat{U}_0 \left\{ \left(r - \frac{D^2}{4r}\right) + \frac{D}{(1+i)\,\alpha r} + \frac{2}{(1+i)\,\alpha}\,e^{-(1+i)\,\alpha n} \right\} \sin\theta\, e^{i\omega t},$$

which is the same as a corresponding expression given by Wang (1968).

The pressure force on the body to $O(\beta^{-\frac{1}{2}})$ is obtained from the two irrotational parts of the flow field W_0 and W_1, since (A 1) shows that the boundary-layer velocity $(q_1 - q_{e0})$ gives no contribution to the surface pressure to this order.

The force for a general body is most easily obtained from the outer flow potentials using Blasius theorem.

In this case since $K_c \to 0$,

$$\mathscr{F}_0 = -j\rho \frac{\partial}{\partial t} \oint_S W_0(z)\,dz,$$

is the zero-order complex force. The streamwise component of this $F_0 = i\omega\rho \hat{U}_0 A C_{M0}$ for a body of cross-sectional area A. However the Blasius formula is only correct for a complex potential W for which the stream function $\mathrm{Im}\,(W)$ is a constant on the body surface. Therefore in the present case the $O(\beta^{-\frac{1}{2}})$ force is given by

$$\mathscr{F}_1 = -j\rho \frac{\partial}{\partial t} \oint_S W_1(z)\,dz - \rho \frac{\partial}{\partial t} \oint_S \mathrm{Im}\{W_1(z)\}\,dz.$$

Since W_1 is a potential derived from a singularity distribution entirely on the body the contour for the first integral may be expanded to infinity. Therefore substituting in both integrals:

$$\mathscr{F}_1 = \frac{-ij\rho\omega}{\pi(1+i)\,\alpha} \oint_\infty \left(\oint_S \frac{d\hat{q}_{e0}}{ds} \log(z - z'(s))\,ds \right) dz - \frac{i\rho\omega}{(1+i)\,\alpha} \oint_S \hat{q}_{e0}\,dz.$$

Since, as $z \to \infty$, $\log(z - z'(s)) = \log(z) - z'/z + \ldots$ and $\oint (d\hat{q}_{e0}/ds)\,ds \equiv 0$, application of the residue theorem gives

$$\mathscr{F}_1 = \frac{-2i\rho\omega}{(1+i)\,\alpha} \oint_S \frac{d\hat{q}_{e0}}{ds} z'(s)\,ds - \frac{i\rho\omega}{(1+i)\,\alpha} \oint_S \hat{q}_{e0}\,dz.$$

After integrating by parts

$$\mathscr{F}_1 = \frac{i\rho\omega}{(1+i)\,\alpha} \oint_S \hat{q}_{e0}\,dz,$$

giving a streamwise force

$$\mathscr{F}_1 = \frac{i\rho\omega}{(1+i)\,\alpha} \oint_S \hat{q}_{e0}\,dx.$$

This is the $O(\beta^{-\frac{1}{2}})$ force induced by pressure on the body surface. However the $(q_1 - q_{e0})$

rotational part of the flow field generates a surface shear stress which also contributes to the overall force,

$$\tau_{\mathrm{W}} = \mu \frac{\partial^2 q_1}{\partial n^2} = -\mu(1+\mathrm{i})^2 \alpha^2 \hat{q}_{\mathrm{e}0}\, \mathrm{e}^{\mathrm{i}\omega t}.$$

Integrating τ_{W} round the surface S gives a total skin-friction force in the streamwise direction

$$\hat{F}_{\mathrm{S}} = \frac{\mathrm{i}\rho\omega}{(1+\mathrm{i})\,\alpha} \oint_S \hat{q}_{\mathrm{e}0}\, \mathrm{d}x.$$

Thus, as in the case of the circular cylinder, the skin-friction and pressure forces due to the boundary layer on a body of arbitrary cross-section to $O(\beta^{-\frac{1}{2}})$ are equal.

The total streamwise force due to the boundary layer is therefore

$$\hat{F}_{\mathrm{BL}} = (1+\mathrm{i})\,\rho\omega D \oint_S \hat{q}_{\mathrm{e}0}\, \mathrm{d}x, \tag{A 2}$$

giving equal contributions in phase with the acceleration and with the velocity.

REFERENCES

Batchelor, G. K. 1967 *An Introduction to Fluid Dynamics*. Cambridge University Press.

Bearman, P. W. & Graham, J. M. R. 1979 Forces on cylinders in harmonically oscillating flow. In *Proc. 2nd Intl Conf. on Behaviour of Off-Shore Structures, London*, pp. 309–322. B.H.R.A. Fluid Engineering, Cranfield, UK.

Bearman, P. W., Graham, J. M. R., Naylor, P. & Obasaju, E. 1981 The role of vortices in oscillatory flow about bluff cylinders. In *Proc. Intl Symp. on Hydrodynamics in Ocean Engng, Trondheim, Norway, August*, pp. 621–635. Norwegian Hydrodynamic Laboratories, Trondheim, Norway.

Drossopoulos, G. M. 1980 On the effects of corner radius on cylindrical bodies in sinusoidally oscillating flow. MSc thesis, University of London.

Graham, J. M. R. 1980 The forces on sharp-edged cylinders in oscillatory flow at low Keulegan–Carpenter numbers. *J. Fluid Mech.* **97**, 331–346.

Graham, J. M. R. 1981 Viscous effects on cylinders at low Keulegan–Carpenter numbers. *London Centre for Marine Technology Fluid Loading Report* FL32.

Grass, A. J. & Kemp, P. H. 1979 Flow visualization studies of oscillatory flow past smooth and rough circular cylinders. In *Mechanics of Wave-Induced Forces on Cylinders* (ed. T. L. Shaw), pp. 437–449. Pitman.

Keulegan, G. H. & Carpenter, L. H. 1958 Forces on cylinders and plates in an oscillating fluid. *J. Res. Nat. Bur. Standards* **60**, 423–440.

Morison, J. R., O'Brien, M. P., Johnson, J. W. & Schaf, S. A. 1950 The force exerted by surface waves on piles. *Petroleum Trans.* **189**, 149–157.

Sarpkaya, T. 1976 Vortex shedding and resistance in harmonic flow about smooth and rough circular cylinders at high Reynolds numbers. *Tech. Report No.* NPS-59SL76021, *Naval Postgraduate School, Monterey, CA.*

Sarpkaya, T. 1981 A critical assessment of Morison's equation. In *Proc. Intl Symp. on Hydrodynamics in Ocean Engng, Trondheim, Norway, August*, pp. 447–467. Norwegian Hydrodynamic Laboratories, Trondheim, Norway.

Sarpkaya, T. & Isaacson, M. 1981 *Mechanics of Wave Forces on Offshore Structures*. New York: Van Nostrand Reinhold.

Singh, S. 1979 Forces on bodies in oscillatory flow. Ph.D. thesis, University of London.

Stokes, G. G. 1851 On the effect of the internal friction of fluids on the motion of pendulums. *Trans. Camb. Phil. Soc.* **9**, 8–106.

Stuart, J. T. 1963 Unsteady boundary layers. In *Laminar Boundary Layers* (ed. L. Rosenhead). Clarendon.

STUART, J. T. & WOODGATE, L. 1955 Experimental determination of the aerodynamic damping on a vibrating circular cylinder. *Phil. Mag.* **46** (7), 40–46.

WANG, C.-Y. 1968 On high-frequency oscillating viscous flows. *J. Fluid Mech.* **32**, 55–68.

WILLIAMSON, C. H. K. 1982 Cylinders in unsteady flow. PhD. Thesis, Dept. of Engineering, Cambridge University.